

1 **On transition-zone water clouds**

2

3 **Eitan Hirsch<sup>1,2</sup>, Ilan Koren<sup>1</sup>, Zev Levin<sup>3,4</sup>, Orit Altaratz<sup>1</sup>, and Eyal Agassi<sup>2</sup>**

4

5 <sup>1</sup>Department of Earth and Planetary Sciences, Weizmann Institute of Science,  
6 Rehovot 76100, Israel

7 <sup>2</sup>Department of Environmental Physics, Israel Institute for Biological Research, Nes-  
8 Ziona, Israel

9 <sup>3</sup>Department of Geophysical, Atmospheric and Planetary Sciences, Tel-Aviv  
10 University, Tel-Aviv, Israel

11 <sup>4</sup>The Energy, Environment and Water Research Center (EEWRC), The Cyprus  
12 Institute, Nicosia, Cyprus

13

14 *Correspondence to:* I. Koren (ilan.koren@weizmann.ac.il)

15

16

1    **Abstract**

2    A recent field campaign was conducted to measure the properties of thin, warm,  
3    convective clouds forming under conditions of weak updrafts. During the campaign,  
4    short-lived clouds (on the order of minutes) with droplets' effective radius of 1–2  $\mu\text{m}$   
5    and low liquid water path ( $\sim 500 \text{ mg m}^{-2}$ ) were measured. These low values are  
6    puzzling, since in most studies an effective radius of 4  $\mu\text{m}$  is reported to serve as the  
7    lower bound for clouds. A theoretical cloud model designed to resolve the droplet-  
8    activation process suggested conditions that favor the formation of such clouds. Here  
9    we show that these clouds, which mark the transition from haze to cloud, are highly  
10   sensitive to the magnitude of the initial perturbation that initiated them. We define  
11   these clouds as “transition-zone clouds”. The existence of such clouds poses a key  
12   challenge for the analysis of atmospheric observations and models, since they “further  
13   smooth” the transition from dry aerosol through haze pockets to cumulus clouds.

14

15

16

1    **1 Introduction**

2

3    Although extensively studied for decades, there is no clear definition of a cloud.  
4    Clouds are often defined by thresholds that depend on the measurement technique  
5    and application, such as the cloud optical depth (COD) threshold when using remote-  
6    sensing tools, or the liquid water content (LWC) threshold in cases of in-situ  
7    measurements and cloud numerical models. Such thresholds are not robust; they  
8    have been shown to misclassify the atmosphere and to introduce problems in  
9    analyses of both cloud and cloud-free regions (Koren et al., 2007, Charlson et al.,  
10   2007). On the micro-scale, the definition of a cloud droplet is more robust, since it is  
11   based on the clear physical discrimination between cloud and haze droplets,  
12   according to the Köhler theory (Kohler, 1936). A droplet that is large enough to grow  
13   spontaneously under environmental supersaturation is considered an activated  
14   cloud droplet. An inactivated droplet, which has not passed the thermodynamic  
15   barrier, is considered a haze droplet. Despite the absence of a clear definition for  
16   clouds, there is general agreement that a substantial number of a cloud's droplets  
17   are activated. For example, continental subarctic low-level clouds have been found  
18   to contain an average fraction of activation of 47 % (with respect to number size  
19   distribution), with variations between 9 % and 86 % (Komppula et al., 2005).

20   There have been many studies on the temporal evolution of haze and cloud droplets  
21   (Mason and Chein, 1962, Mordy, 1959 and Reutter et al., 2009). The presence of  
22   these two thermodynamic states, controlled by the degree of supersaturation,  
23   suggests an interesting evolution of the droplets' size-distribution function. Whereas  
24   haze is in a stable equilibrium, activated droplets are in an unstable equilibrium and

1 their growth rate is inversely proportional to their radii. Such a diffusional growth  
2 rate dictates faster radial growth of small vs. bigger activated droplets. It has been  
3 shown that activated droplets in an ascending parcel reach a radius of more than 6  
4  $\mu\text{m}$  in less than 100 s, regardless of their initial size (Mordy, 1959). Therefore, the  
5 time during which the effective radius of the cloud droplet distribution is 1 – 3  $\mu\text{m}$  is  
6 very short, and the likelihood of a cloud to obtain such an effective radius is very  
7 small. On the other hand, the differences in drop growth rates become negligible as  
8 they grow. The growth rate of activated droplets with radius larger than 10  $\mu\text{m}$   
9 depends mainly on the degree of supersaturation, rather than their size (Rogers,  
10 1979). These properties create two droplet size gathering foci. One below the Köhler  
11 maxima that contains the haze particles, and the second one drifting toward the  
12 larger end of the spectrum of the growing activated droplets. Therefore, since the  
13 effective radius is biased toward the larger droplets, its value will usually be bigger  
14 than 1 – 3  $\mu\text{m}$ . These considerations explain why a threshold radius of 4  $\mu\text{m}$  is often  
15 used as the lowest value that can represent a cloud (Kawamoto et al., 2001), and  
16 why an effective radius in the range of 1 – 3  $\mu\text{m}$  is considered transient, resulting in a  
17 small likelihood of capturing it for most cumulus clouds. These estimations agree  
18 well with observational records of effective radii of clouds. Extensive in-situ  
19 measurements (Miles et al., 2000) of global marine and continental low-level  
20 stratiform clouds gave a mean effective radius ( $r_{\text{eff}}$ ) of  $9.6 \pm 2.35 \mu\text{m}$  and  $5.4 \pm 2.05$   
21  $\mu\text{m}$ , respectively. In addition, a nearly global survey of the effective radii in marine  
22 and continental shallow warm clouds (Han et al., 1994) indicated mean  $r_{\text{eff}}$  values of  
23 11.8  $\mu\text{m}$  and 8.5  $\mu\text{m}$ , respectively. Nevertheless, small  $r_{\text{eff}}$  values, in the range of 3.5  
24 – 5.5  $\mu\text{m}$ , have been reported for in-situ measurements of continental boundary

1 layer cumulus clouds (Han et al., 1995, Vogelmann et al., 2012). These values  
2 coincide well with the findings of Deng et al. (2009) who reported an average  $r_{\text{eff}}$  of  
3  $3.86 \mu\text{m}$ , with an average LWC of  $0.16 \text{ g m}^{-3}$ , from in-situ measurements of Cu clouds  
4 in Beijing. The smallest  $r_{\text{eff}}$  values were reported by Reid et al. (1999), who studied  
5 the properties of warm convective clouds in Brazil by in-situ measurements, and  
6 documented  $r_{\text{eff}}$  readings of  $2 \mu\text{m}$  in a highly polluted environment. In addition, they  
7 provided a mathematical connection between the  $r_{\text{eff}}$  and the LWC which could  
8 explain 70 % of the variance in the measured data. Furthermore, in another study, a  
9 relationship between the liquid water path (LWP) and the  $r_{\text{eff}}$  of a cloud was found  
10 (Liu et al., 2003), suggesting that a small  $r_{\text{eff}}$  is positively correlated with small LWP.

11 During the Eastern Mediterranean summer, it is typical to find stagnant atmospheric  
12 conditions, with a moist boundary layer and a near-neutral lapse rate that is  
13 bounded by an inversion layer. Since in many cases, the lifting condensation level  
14 (LCL) is located above the inversion layer, standard forecasting tools predict no  
15 clouds formation at these days.

16 In this study, we focus on the very small end of the size distribution of convective  
17 clouds. During a recent field campaign (see next section for further details), we  
18 measured many short-lived Cu clouds (see an example in Fig. 1) that were  
19 characterized by very small  $r_{\text{eff}}$  values. Our study raises several questions: Are these  
20 clouds? According to which definition can we identify them as clouds (remote  
21 sensing, modeling, microphysical)? Using theoretical cloud equations together with  
22 observations, we study the properties of this unique subset of clouds.

23



1      Figure 1 - Images taken during a field campaign on 30 June 2011 at 15:52–15:56 LT.  
2  
3      Top: sequential (1-min time lag) images of the complete lifetime of a single short-  
4      lived cloud. The camera was pointed at the zenith and the diagonal field of view is  
5      180°. The yellow rectangles mark the position of the cloud. Bottom: enlargement of  
6      one of the images.

7  
8  
9

10     **2 Methods**

11     A field campaign was conducted during the summer (June–August) of 2011 in Israel,  
12     focusing on the microphysical and optical properties of thin, warm convective  
13     clouds. The measurement site was in Nes-Ziona, which is located approximately 10

1 km away from the coast. The cloud properties were retrieved using a novel ground-  
2 based hyperspectral technique (Hirsch et al., 2012) which was developed to retrieve  
3 the optical (COD) and microphysical ( $r_{\text{eff}}$ , LWP) properties of thin, warm clouds. It  
4 relies on three elements: detailed radiative-transfer calculations in the longwave-IR  
5 regime, signal enhancement by subtraction of a clear sky reference, and a spectral  
6 matching method that exploits fine spectral differences between water droplets of  
7 different radii. The sensors were pointed to the zenith and the measurements were  
8 conducted at a rate of 0.5 Hz, thus the COD,  $r_{\text{eff}}$  and LWP were derived every 2 s.  
9 Since the retrieval is based on spectral analysis, its accuracy is not constant for all  
10 values of  $r_{\text{eff}}$ . However, the retrieval is at its highest sensitivity for thin clouds, and  
11 the error is estimated to be  $\pm 0.5 \mu\text{m}$  for  $r_{\text{eff}} \approx 2 \mu\text{m}$  and for  $\text{LWP} < 10 \text{ g m}^{-2}$  (see Hirsch  
12 et al, 2012 for further details).

13 Complementary measurements of the atmospheric profile and cloud base height  
14 were conducted by the Israel Meteorological Service (IMS) at Beit-Dagan station,  
15 which is located 10 km north of the cloud-measurement system, in a similar distance  
16 from the coast. Thus, the influence of the sea breeze on the atmospheric conditions  
17 at both sites is expected to be similar. The cloud base height was measured by  
18 ceilometer, and the atmospheric conditions were measured twice a day by a  
19 radiosonde (at 0:00 UTC and 12:00 UTC). The data were downloaded from the  
20 University of Wyoming website (Website: Atmospheric sounding). The radiosonde  
21 provides information on temperature, pressure, humidity, and horizontal wind speed  
22 profiles from the surface to the end of the troposphere. As explained later, the daily  
23 12:00 UTC atmospheric profiles were used as an input data for the theoretical cloud  
24 model and for calculating the expected cloud-base height (based on LCL). Those

1 values were compared to the measured cloud base height at the same geographical  
2 location, at Beit-Dagan.

3 To examine the atmospheric conditions under which such clouds can form, a  
4 theoretical cloud model was developed. We used the basic cloud physics equations  
5 to investigate air-parcel evolution under weak updraft conditions, below a thermal  
6 inversion (see Appendix A for a comprehensive description of the parcel model).

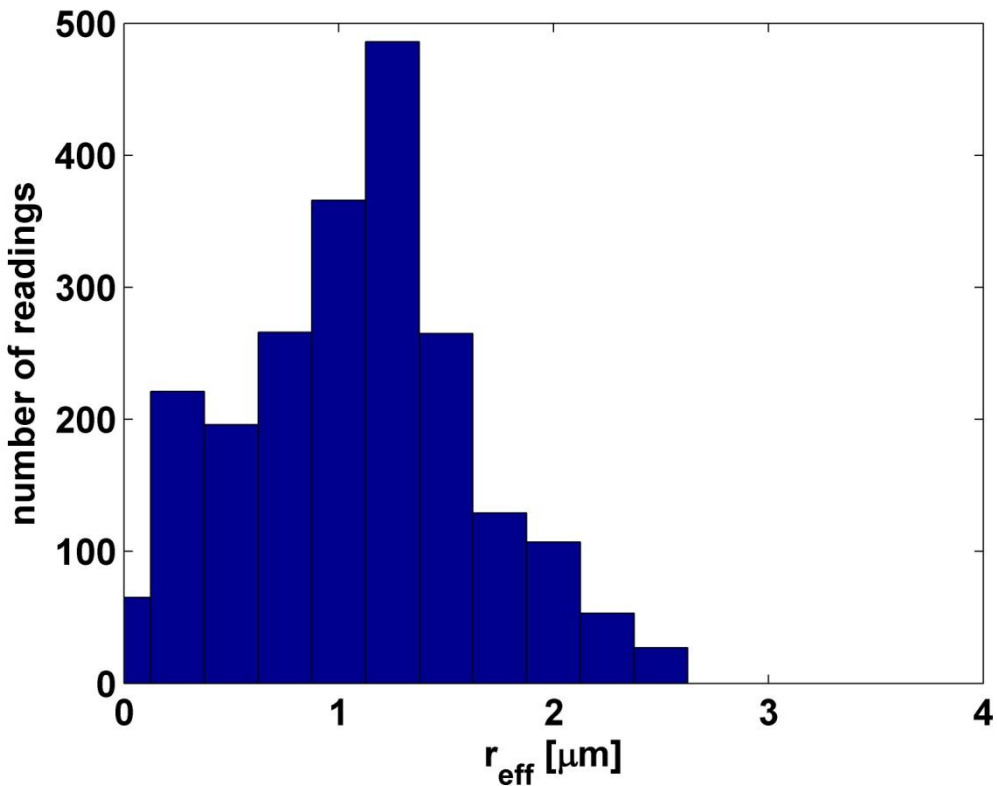
7 There are parcel models that use conserved thermodynamic parameters such as  
8 potential temperature or equivalent potential temperature (see for example Berg  
9 and Stull, 2004). However, the purpose of our model was to resolve the parcel  
10 motion and to enable detailed analysis of the uptake of water vapor by haze droplets  
11 and of droplets activation process. The model solves the first law of thermodynamics  
12 directly. As detailed in Appendix A, the cloud model accounts for the effect of  
13 entrainment only on the momentum. However, under the specific conditions of  
14 relatively weak updrafts, which serve as the "entrainment engine", such  
15 representation provides a reasonable approximation. Moreover, the coupling  
16 between the model's equations imposes interaction of the entrainment process with  
17 all other processes.

18 The droplet  $r_{\text{eff}}$  and supersaturation within the parcel, as well as the cloud's updraft  
19 and LWC were calculated for a range of initial conditions. The 24 dry aerosol size  
20 distributions used in the model were measured in situ in Europe and in the  
21 Mediterranean (Asmi et al., 2011), and the aerosols were assumed to be ammonium  
22 sulfate.

23

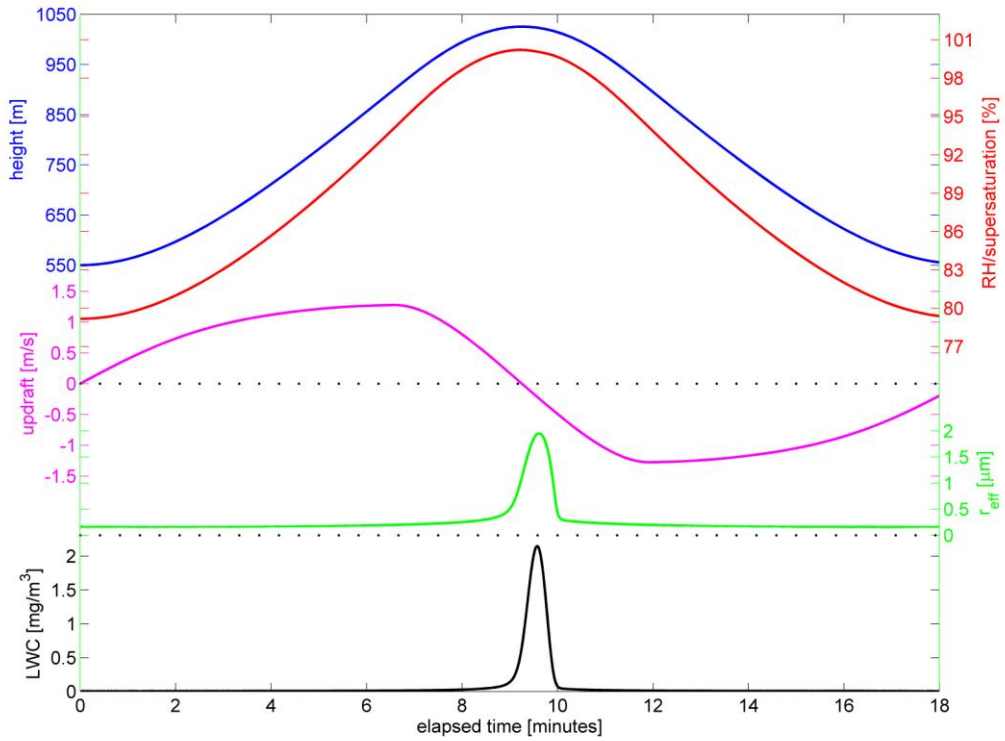
24 **3 Results**

1 Here we present a detailed case study of one day in the field campaign (30 June  
2 2011, see the tephigram in Appendix B, Fig. B1). Analysis of the cloud measurements  
3 from that day revealed many short-lived clouds with uncommonly small  $r_{\text{eff}}$ . An  
4 example of one specific cloud is presented in Fig. 1. The cloud appears ordinary to  
5 the naked eye, and it has a short lifetime of only 6 min. Use of the retrieval method  
6 revealed the COD, LWP and  $r_{\text{eff}}$  as the cloud passed above the sensors in the zenith.  
7 The temporal average  $r_{\text{eff}}$  of the cloud (as it passed in the zenith) was  $1.24 \mu\text{m}$  (with  
8 standard deviation of  $\sigma = 0.2 \mu\text{m}$ ), the average LWP was  $0.13 \text{ g m}^{-2}$  (with  $0.01 \text{ g m}^{-2}$   
9 and  $0.37 \text{ g m}^{-2}$  as the 10<sup>th</sup> and 90<sup>th</sup> percentiles respectively), and the average COD at  
10 550 nm was 9.15 (with 0.66 and 30.3 as the 10<sup>th</sup> and 90<sup>th</sup> percentiles respectively).  
11 The data collected on this day showed many more clouds with similar characteristics.  
12 Most of the  $r_{\text{eff}}$  readings during noontime of that day were smaller than  $2 \mu\text{m}$  (Figure  
13 2) and the clouds had a relatively short lifetime (several minutes at most).



1 Figure 2. A histogram of effective radius ( $r_{\text{eff}}$ ) readings from 14:00–16:00 LT on 30  
 2 June 2011. Most of the  $r_{\text{eff}}$  readings are below 2  $\mu\text{m}$ . Data were measured at a rate of  
 3 0.5 Hz.  
 4  
 5 Based on the sounding data from the Beit-Dagan meteorological station measured  
 6 on 30 June 2011 at 12:00 UTC (15:00 LT), we simulated the formation of thin warm  
 7 clouds on that day. The dry aerosol number size distribution that was used is based  
 8 on measured aerosol size spectra from the island of Crete, and the diameters can be  
 9 represented as a sum of two log-normal distributions centered at 86 and 189 nm  
 10 (see full description in Asmi et al, 2011, station FKL). A wide range of RH  
 11 perturbations and initial vertical locations were used (presented in more detail  
 12 further on). Figure. 3 shows an example of one simulation of the formation of a  
 13 small, warm cloud. To initiate the cloud formation we used a RH perturbation of 11  
 14 % above ambient RH (68 %), at a height of 550 m. The initial updraft of the parcel

1 was set to zero, and its temperature was equal to the ambient temperature at that  
2 level ( $20.1^{\circ}\text{C}$ ). Examination of Figure. 3 reveals that the parcel rose  $\sim 475$  m and  
3 reached a low supersaturation of  $\sim 0.2\%$ , along with a LWC of  $2.15 \text{ mg m}^{-3}$ . The  
4 maximal  $r_{\text{eff}}$  of the droplets was  $1.95 \mu\text{m}$ , while the parcel drifted up with a weak  
5 updraft (average of  $86 \text{ cm s}^{-1}$ ), reaching a maximal value of  $128 \text{ cm s}^{-1}$  for a very  
6 short time (see Figure. 3). It is interesting to note the time lag between the maximal  
7 updraft and maximal LWC. At the stage of maximal updraft, the parcel contains only  
8 haze droplets, none of its droplets are activated and it is subvisual to the naked eye.  
9 When the parcel reaches its maximal LWC (and supersaturation), the updraft is  
10 completely exhausted, it turns into a downdraft and the cloud is already in the  
11 dissipation stage.



1

2 Figure. 3. Temporal evolution of an air parcel. Vertical position (blue), relative  
 3 humidity (RH) and supersaturation (red), updraft (magenta), effective radius ( $r_{\text{eff}}$ ),  
 4 green), and liquid water content (LWC, black).

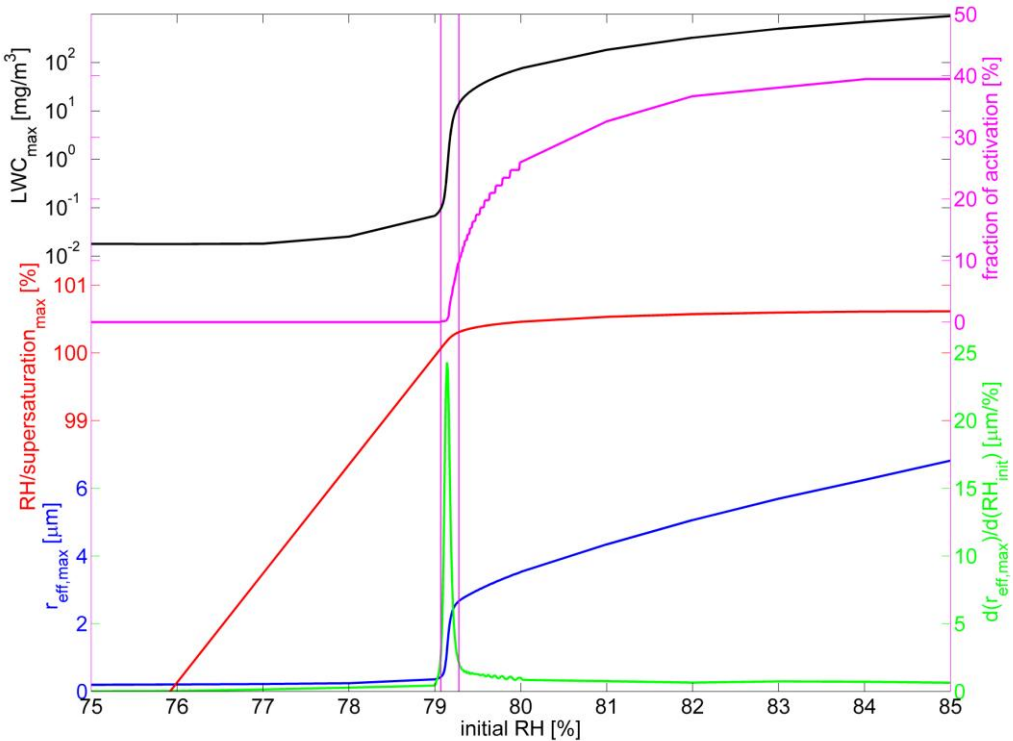
5

6 The dependency of the cloud's properties on the initial RH of the parcel was  
 7 examined and the results are presented in Figure 4. The ambient RH was 68 % and  
 8 the perturbations ranged between 7 and 17 %. Every point in the figure represents  
 9 the results of a complete simulation, similar to the one presented in Figure. 3, using  
 10 the same dry aerosol size distribution (based on measurements from Crete, Asmi et  
 11 al, 2011). The maximal  $r_{\text{eff}}$  (blue), maximal RH (red), and maximal LWC (black) of the  
 12 forming clouds were plotted against the initial RH of the parcel. In addition, the  
 13 fraction of activated droplets (in terms of number size distribution) is plotted against  
 14 the initial RH (magenta). To emphasize the dependency of the maximal  $r_{\text{eff}}$  on initial

1 RH, we plotted the derivative of the blue line ( $r_{\text{eff,max}}$ ) against  $\text{RH}_{\text{init}}$   
2 ( $d(r_{\text{eff,max}})/d(\text{RH}_{\text{init}})$ , in green). We defined the cases with  $d(r_{\text{eff,max}})/d(\text{RH}_{\text{init}}) > 2 \mu\text{m } \text{‰}^{-1}$   
3 as "transition-zone" clouds (marked with vertical magenta lines). The clear and  
4 narrow transition zone seen in all of the graphs ( $r_{\text{eff}}$ , RH and LWC) implies that these  
5 clouds are highly sensitive to the initial conditions of the parcel. Furthermore, it  
6 reinforces the common assumption of a minimal  $r_{\text{eff}}$  of 4  $\mu\text{m}$  for clouds, located well  
7 beyond the transition zone.

8 Although the marked region appears small, it does not necessarily represent the  
9 likelihood of such conditions in nature; in fact, it represents a wide range of possible  
10 values. The range of the maximal  $r_{\text{eff}}$  is from 0.43 to 2.67  $\mu\text{m}$ , while the range of the  
11 maximal LWC is between 0.1 and 14.1  $\text{mg m}^{-3}$ . In addition, maximal supersaturation  
12 ranges between 0.07 and 0.31 %, whereas the average updraft is approximately  
13 constant at 0.86  $\text{m s}^{-1}$ . It is also interesting to note that the maximal fraction of  
14 activation can be in some clouds lower than 10 % (in terms of number size  
15 distribution), which is the lower limit that can be measured in cumulus clouds  
16 (Komppula et al., 2005).

17 Furthermore, it is possible to define a criterion for the cloud's lifetime. For every  
18 simulated cloud, we defined its lifetime as the period during which the  $r_{\text{eff}}$  exceeds  
19 0.5  $\mu\text{m}$ . This threshold was chosen since it represents the beginning of the droplets  
20 activation process in clouds. For the clouds that appear in Figure 4, when the  
21 maximal  $r_{\text{eff}}$  reaches 0.5  $\mu\text{m}$ , the fraction of activation (in terms of number size  
22 distribution) is 0.13 %. Using this definition, the range of possible lifetimes spans up  
23 to 1.4 min.



1

2 Figure 4. The maximal effective radius ( $r_{\text{eff}}$ , blue), maximal relative humidity (RH, red), maximal liquid water content (LWC, black), and fraction of activation (in terms 3 of number size distribution, magenta) of the forming clouds vs. the initial RH of the 4 parcel. The green line is the derivative of the maximal  $r_{\text{eff}}$  with respect to the initial 5 RH of the parcel. Transition-zone clouds are defined within the vertical magenta lines 6 (see text for further explanation).

7

8

9 Further examination of the model results for a range of different initial vertical 10 locations of the parcel and initial RH values, revealed a range of possible values for 11 the microphysical properties and lifetimes of the formed clouds. In every panel in 12 Figure 5, the temperature (blue) and RH (red) profiles are plotted along with the 13 ceilometer measurement of cloud-base height (horizontal blue line) and the 14 theoretical LCLs (horizontal cyan and magenta lines). As detailed in Appendix A, One

1 of the LCL calculations was based on a ground-level ascending parcel and the other  
2 on a parcel with average properties of the lowest 500 m. First, we note that the  
3 measured cloud base is ~500 m below the LCL (both cloud base and atmospheric  
4 profile-for estimating LCL were measured in Beit Dagan). According to the cloud  
5 model results, only parcels that initiated at altitudes between 250 and 750 m formed  
6 a cloud base height that is comparable with the actual measured one. Therefore,  
7 only those parcels results are presented. In Figure 5a, the lower symbol of every pair  
8 of symbols represents both the initial height of the parcel and the size of the  
9 smallest RH perturbation that created a cloud (determined by a threshold of RH >  
10 100 %). The higher symbol of every pair represents the simulated cloud-base height.  
11 It can be noticed that all the parcels that originated between 250 - 750 m created  
12 clouds with similar base heights that are comparable with the measured value.

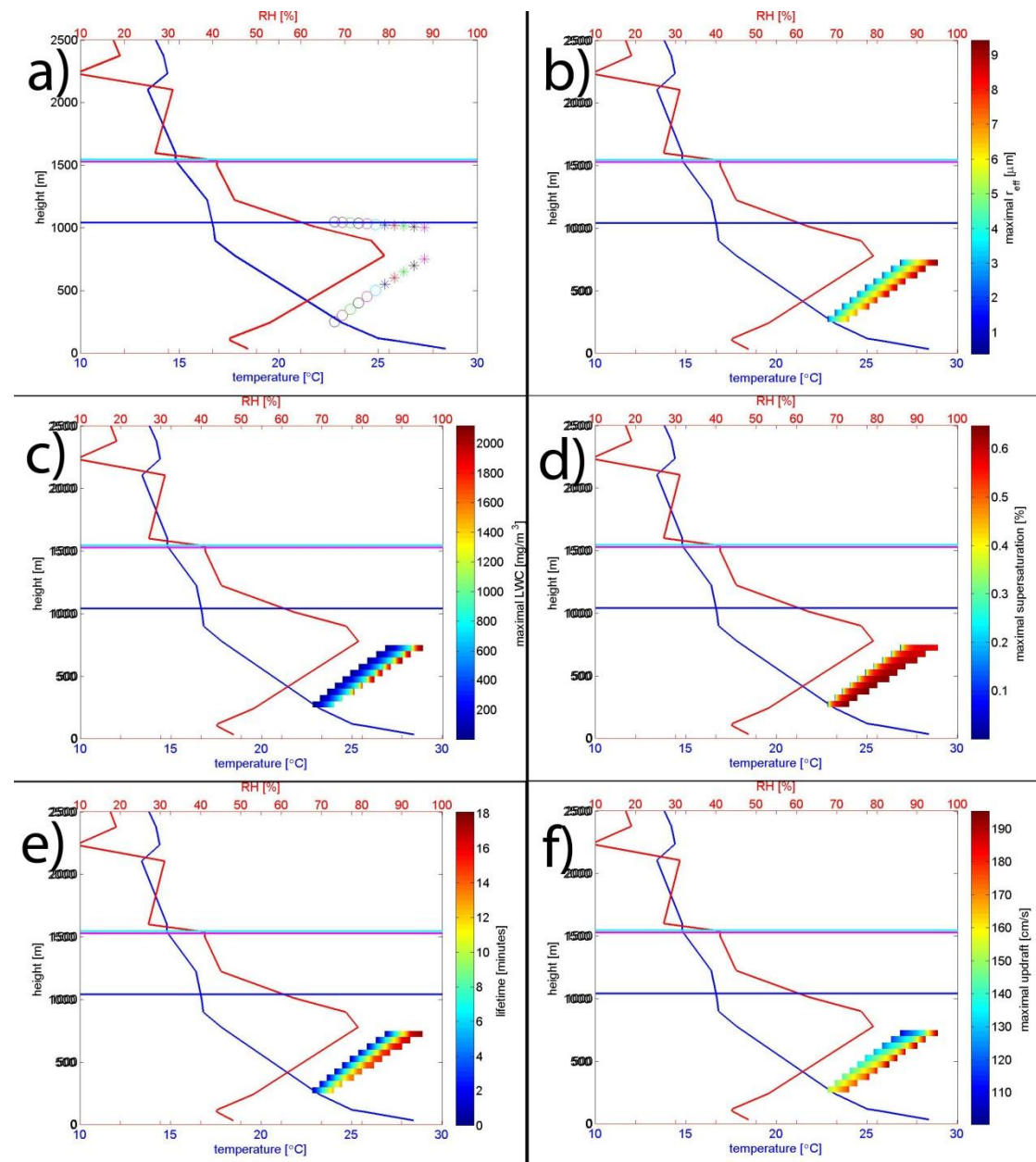
13 Figure 5b–f presents the possible values of maximal  $r_{eff}$ , maximal LWC, maximal  
14 supersaturation, lifetime, and average updraft, respectively. The colored region  
15 corresponds to the value of the simulated parameter. The position of the colored  
16 region on the graph represents the initial height of the parcel and the magnitude of  
17 the RH perturbation, i.e. the difference between the lower colored region and the  
18 red line represents the perturbation in the RH.

19 By analyzing the results presented in Figure. 5 and following the definition of  
20 transition-zone clouds, it is possible to calculate the possible supersaturation, LWC  
21 and  $r_{eff}$  values of those clouds, while considering different heights from which the  
22 parcel might have started to ascend. The maximal  $r_{eff}$  varies between 0.41 and 2.69  
23  $\mu\text{m}$ , while the maximal LWC ranges between 0.09 and  $16.8 \text{ mg m}^{-3}$ . The maximal  
24 supersaturation varies between 0.05 and 0.33 % and the average updraft ranges

1 between 0.62 and 1.15 m s<sup>-1</sup>. When considering the possible initial heights of the  
 2 parcel, the lifetime of the transition-zone clouds may reach 13.5 min, but it is often  
 3 much shorter.

4

5

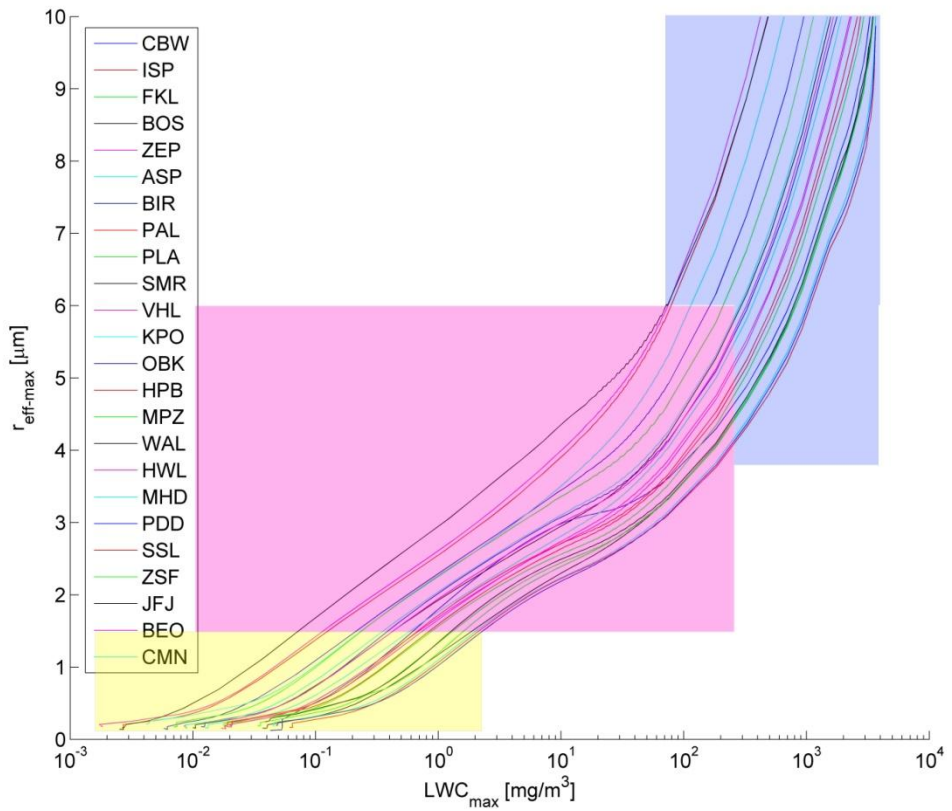


7 Figure. 5. Theoretical cloud model results for a range of possible initial heights and  
 8 relative humidity (RH) perturbations for the atmospheric profile of 30 June 2011,

1 12:00 UTC. **(a)** The lower symbol of every pair of symbols represents both the initial  
2 height of the parcel and the size of the smallest RH perturbation that created a cloud  
3 (determined as  $\text{RH} > 100\%$ ). The higher symbol of every pair represents the  
4 simulated cloud-base height. Note that all of the simulated parcels (initial heights  
5 250 – 750 m) resulted in a cloud base at the measured value (horizontal blue line).  
6 **(b)** Possible values of the maximal effective radius ( $r_{\text{eff}}$ ) for different initial heights  
7 and different perturbations. The colored region corresponds to the value of the  
8 simulated maximal  $r_{\text{eff}}$ . The position of the colored region on the graph represents  
9 the initial height of the parcel and the magnitude of the RH perturbation. **(c–f)** Same  
10 as panel (b) but for maximal liquid water content (LWC), maximal supersaturation,  
11 lifetime, and average updraft, respectively.

12  
13 How sensitive are these results to the aerosol model? To study the effect of dry  
14 aerosol size distribution on the properties of the forming clouds, we used 24 types of  
15 dry aerosol size distributions that had been measured in situ in Europe and the  
16 Mediterranean region (Asmi et al., 2011). Figure. 6 demonstrates that the  
17 phenomenon of transition-zone clouds is independent of the dry aerosol size  
18 distribution, although the microphysical properties (LWC, supersaturation,  $r_{\text{eff}}$ ) of  
19 the forming clouds are affected. Figure. 6 presents a group of curves representing  
20 the results of 3,192 different simulations for 24 types of dry aerosol size distributions  
21 (every distribution with 133 different initial RH perturbations). The maximal  $r_{\text{eff}}$  of  
22 the droplets is presented vs. the maximal LWC in the cloud. All parcels were initiated  
23 at a height of 550 m, while every point on the curves represents a full simulation,  
24 similar to the one presented in Figure. 3, for a different initial dry aerosol size

1 distribution and different initial RH perturbations An examination of the curves  
2 shows the regime in this phase space, dominated by "transition-zone" clouds. This  
3 regime is determined based on the presented criterion for recognizing the zone of  
4 sharp change in cloud properties as a function of the initial RH perturbation for  
5 similar dry aerosol distribution simulations (see explanation of Fig. 4). In a  
6 subsaturated air parcel, haze develops with a submicron  $r_{\text{eff}}$  (shaded yellow region).  
7 On the other hand, initial perturbation with relatively high RH compared to the  
8 environment (shaded blue region) can produce more developed clouds that are  
9 characterized by larger  $r_{\text{eff}}$  and higher LWC. In the intermediate zone (shaded  
10 magenta region), transition-zone clouds are formed, namely clouds that are  
11 transitional between haze and Cu clouds. They are, by definition, highly sensitive to  
12 the initial RH perturbation. When considering the wide range of possible dry aerosol  
13 size distributions, the maximal  $r_{\text{eff}}$  may vary between 1.5 and 6  $\mu\text{m}$ , while the  
14 maximal LWC ranges between 0.01 and 73  $\text{mg m}^{-3}$ . The supersaturation can be as  
15 high as 0.6 %, while the average updraft is almost unaffected by the aerosol size  
16 distribution (range of  $0.85 - 0.87 \text{ m s}^{-1}$ ).



1

2 Figure. 6. The maximal effective radius ( $r_{\text{eff-max}}$ ) vs the maximal liquid water content

3 ( $LWC_{\text{max}}$ ) in the cloud for different dry aerosol size distributions (Asmi et al., 2011)

4 and different initial relative humidity perturbations. Each line represents a different

5 dry aerosol size distribution. The labels follow the names given by Asmi et al. (2011).

6 The different shaded regions represent conditions of haze (subsaturation, yellow),

7 transition-zone clouds (magenta), and more developed Cu clouds (blue).

8

9 Obviously, the occurrence of transition-zone clouds is not restricted to the eastern

10 Mediterranean region. Similar atmospheric conditions are quite common during the

11 summer in other locations around the globe (specifically coastal areas along the

12 subtropical belt), in which a persistent synoptic-scale subsidence exists. In such

1 places, it is common to see small (on the scale of 100 m) cumulus clouds that form  
2 and dissipate within a few minutes.

3

4 **4 Summary and discussion**

5

6 In this study, we focused on a cloud regime that is usually overlooked. Observational  
7 evidence for warm clouds with small  $r_{\text{eff}}$ , small LWP, and a short lifetime were found  
8 during a field campaign. These observations initiated a detailed analysis using a bin  
9 microphysics cloud model to study the microphysical properties of small, short-lived  
10 convective clouds under weak updrafts regime in a humid boundary layer bounded  
11 by a thermal inversion. The model predicts that under such conditions, a special  
12 subset of clouds with unique microphysical properties can form. Such clouds are  
13 defined here as transition-zone clouds because their thermodynamic state is in the  
14 transition between haze and cumulus clouds. They are highly sensitive to the initial  
15 perturbation, and they are characterized by a  $r_{\text{eff}} < \sim 3 \mu\text{m}$ , which is conventionally  
16 considered below the threshold of cumulus clouds. Such clouds contain a relatively  
17 low LWC ( $< 17 \text{ mg m}^{-3}$ ), and have a small COD. In addition, these clouds reach their  
18 maximal LWC when their driving updraft has already dissipated. There is a possibility  
19 that the atmospheric conditions at the measurement site (at Nes Ziona) where the  
20 clouds characteristics were measured, were different from the atmospheric profiles  
21 measured in Beit Dagan station, but due to the similar distances of both stations  
22 from the sea shore it is not plausible.

23 Because of their temporal and spatial properties, such clouds are likely to escape the  
24 scientific “cloud radar”. Small, short-lived clouds form a collective suite of challenges

1 to study. Their physical properties fall below most of the sampling rate and  
2 sensitivity limits of in-situ measurement instruments, and are smaller than the  
3 spatial resolution of most climate-oriented remote sensing sensors. Moreover, most  
4 of the RH measurement techniques are limited to a lower supersaturation bound of  
5 0.2 % (Snider et al., 2003); and measurements of low supersaturation are difficult to  
6 perform and are usually highly inaccurate (Rose et al., 2008). It is therefore quite  
7 hard to characterize these clouds.

8 This study raises several interesting and important issues regarding the way in which  
9 clouds are defined. Our results can be generalized, suggesting that there are  
10 convective clouds with maximal size in the range of a few hundred meters or less,  
11 that form below an inversion layer, characterized by low supersaturation values.

12 It has already been noted that the region between clouds within a cloud field (also  
13 known as the clouds' twilight zone; Koren et al. 2007) is characterized by unique  
14 optical properties, and that the commonly used discrimination between clear and  
15 cloudy skies might lead to substantial errors in estimating radiative forcing (Charlson  
16 et al, 2007). In this paper, we explore the range of small clouds that lie between haze  
17 and conventional, more developed cumulus clouds, and introduce the transition-  
18 zone cloud. Although these clouds seem to exist for only a relatively small range of  
19 initial conditions, they are expected to be quite common, since they form in  
20 common environmental conditions. Moreover, a link is expected between the  
21 clouds' size and frequency of occurrence (Koren et al., 2008, Wood and Field, 2011,  
22 Zhao and Girolamo, 2007). As these clouds occupy the small end of the Cu cloud size  
23 distribution, their number is the highest. Since previous studies reported cases  
24 where small clouds contributed ~50 % of the reflectance (Koren et al., 2008), these

1 findings suggest that at some environmental conditions the subset of transition-zone  
2 clouds has an important radiative forcing effect which is currently either not  
3 considered, or wrongly attributed to aerosols.  
4 Furthermore, these clouds might better explain the unique optical properties of the  
5 clouds' twilight zone. Our findings suggest that weight should be given to theoretical  
6 studies, as well as to the development of instruments and measuring techniques that  
7 will enable us to advance our knowledge of this important and understudied subset  
8 of clouds.

9

10 **Acknowledgements**

11 The research leading to these results was funded by the European Research Council  
12 under the European Union's Seventh Framework Programme (FP7/2007-2013) /ERC  
13 Grant agreement n° [306965].

14

15 **References**

16 Asmi, A., Wiedensohler, A., Laj, P., Fjaeraa, A.-M., Sellegri, K., Birmili, W.,  
17 Weingartner, E., Baltensperger, U., Zdimal, V., and Zikova, N.: Number size  
18 distributions and seasonality of submicron particles in Europe 2008–2009,  
19 Atmospheric Chemistry and Physics, 11, 5505-5538, 2011.  
20 Atmospheric sounding: <http://weather.uwyo.edu/upperair/sounding.html>, last  
21 access: October 2013.

22 Berg, L. K., R. B. Stull, 2004: Parameterization of Joint Frequency Distributions of  
23 Potential Temperature and Water Vapor Mixing Ratio in the Daytime Convective

1 Boundary Layer. *J. Atmos. Sci.*, 61, 813–828. doi: [http://dx.doi.org/10.1175/1520-0469\(2004\)061<0813:POJFDO>2.0.CO;2](http://dx.doi.org/10.1175/1520-0469(2004)061<0813:POJFDO>2.0.CO;2)

3 Bolton, D.: The Computation of Equivalent Potential Temperature, *Monthly Weather*  
4 *Review*, 108, 1046-1053, 10.1175/1520-0493(1980)108<1046:tcoept>2.0.co;2, 1980.

5 Brooks, S. D., Wise, M. E., Cushing, M., and Tolbert, M. A.: Deliquescence behavior of  
6 organic/ammonium sulfate aerosol, *Geophysical Research Letters*, 29, 1917, 2002.

7 Charlson, R. J., Ackerman, A. S., BENDER, F. A. M., Anderson, T. L., and Liu, Z.: On the  
8 climate forcing consequences of the albedo continuum between cloudy and clear air,  
9 *Tellus B*, 59, 715-727, 2007.

10 Deng, Z., Zhao, C., Zhang, Q., Huang, M., and Ma, X.: Statistical analysis of  
11 microphysical properties and the parameterization of effective radius of warm  
12 clouds in Beijing area, *Atmospheric Research*, 93, 888-896, 2009.

13 Dusek, U., Frank, G., Hildebrandt, L., Curtius, J., Schneider, J., Walter, S., Chand, D.,  
14 Drewnick, F., Hings, S., and Jung, D.: Size matters more than chemistry for cloud-  
15 nucleating ability of aerosol particles, *Science*, 312, 1375-1378, 2006.

16 Han, Q., Rossow, W. B., and Lacis, A. A.: Near-global survey of effective droplet radii  
17 in liquid water clouds using ISCCP data, *Journal of Climate*, 7, 465-497, 1994.

18 Han, Q., Welch, R., Chou, J., Rossow, W., and White, A.: Validation of satellite  
19 retrievals of cloud microphysics and liquid water path using observations from FIRE,  
20 *Journal of the atmospheric sciences*, 52, 4183-4195, 1995.

21 Hirsch, E., Agassi, E., and Koren, I.: Determination of optical and microphysical  
22 properties of thin warm clouds using ground based hyper-spectral analysis,  
23 *Atmospheric Measurement Techniques*, 5, 851-871, 2012.

1 Kawamoto, K., Nakajima, T., and Nakajima, T. Y.: A global determination of cloud  
2 microphysics with AVHRR remote sensing, *Journal of Climate*, 14, 2054-2068, 2001.

3 Köhler, H.: The nucleus in and the growth of hygroscopic droplets, *Transactions of*  
4 *the Faraday Society*, 32, 1152-1161, 1936.

5 Komppula, M., Lihavainen, H., Kerminen, V. M., Kulmala, M., and Viisanen, Y.:  
6 Measurements of cloud droplet activation of aerosol particles at a clean subarctic  
7 background site, *Journal of Geophysical Research: Atmospheres (1984–2012)*, 110,  
8 2005.

9 Koren, I., Remer, L. A., Kaufman, Y. J., Rudich, Y., and Martins, J. V.: On the twilight  
10 zone between clouds and aerosols, *Geophysical research letters*, 34, 2007.

11 Koren, I., Oreopoulos, L., Feingold, G., Remer, L., and Altaratz, O.: How small is a  
12 small cloud?, *Atmospheric Chemistry and Physics*, 8, 3855-3864, 2008.

13 Lee, I.-Y., and Pruppacher, H.: A comparative study on the growth of cloud drops by  
14 condensation using an air parcel model with and without entrainment, *pure and*  
15 *applied geophysics*, 115, 523-545, 1977.

16 Liu, G., Shao, H., Coakley, J. A., Curry, J. A., Haggerty, J. A., and Tschudi, M. A.:  
17 Retrieval of cloud droplet size from visible and microwave radiometric  
18 measurements during INDOEX: Implication to aerosols' indirect radiative effect,  
19 *Journal of Geophysical Research: Atmospheres (1984–2012)*, 108, AAC 2-1-AAC 2-10,  
20 2003.

21 Mason, B., and Chien, C.: Cloud-droplet growth by condensation in cumulus,  
22 *Quarterly Journal of the Royal Meteorological Society*, 88, 136-142, 1962.

23 Miles, N. L., Verlinde, J., and Clothiaux, E. E.: Cloud droplet size distributions in low-  
24 level stratiform clouds, *Journal of the atmospheric sciences*, 57, 295-311, 2000.

1 Mordy, W.: Computations of the growth by condensation of a population of cloud  
2 droplets, *Tellus*, 11, 16-44, 1959.

3 Pruppacher, H. R., Klett, J. D., and Wang, P. K.: *Microphysics of clouds and*  
4 *precipitation*, 1998.

5 Reid, J. S., Hobbs, P. V., Rangno, A. L., and Hegg, D. A.: Relationships between cloud  
6 droplet effective radius, liquid water content, and droplet concentration for warm  
7 clouds in Brazil embedded in biomass smoke, *Journal of Geophysical Research: Atmospheres* (1984–2012), 104, 6145-6153, 1999.

8 Reutter, P., Su, H., Trentmann, J., Simmel, M., Rose, D., Gunthe, S., Wernli, H.,  
9 Andreae, M., and Pöschl, U.: Aerosol-and updraft-limited regimes of cloud droplet  
10 formation: influence of particle number, size and hygroscopicity on the activation of  
11 cloud condensation nuclei (CCN), *Atmospheric Chemistry and Physics*, 9, 7067-7080,  
12 2009.

13 Rogers, R.: *A short course in cloud physics*, Oxford and Elmsford, N. Y., Pergamon  
14 Press (International Series in Natural Philosophy, 96, 246, 1979.

15 Roland, B. S.: *An introduction to boundary layer meteorology*, Boston:  
16 Kluwel'Academic Publishers, 1988.

17 Rose, D., Gunthe, S., Mikhailov, E., Frank, G., Dusek, U., Andreae, M., and Pöschl, U.:  
18 Calibration and measurement uncertainties of a continuous-flow cloud condensation  
19 nuclei counter (DMT-CCNC): CCN activation of ammonium sulfate and sodium  
20 chloride aerosol particles in theory and experiment, *Atmospheric Chemistry and*  
21 *Physics*, 8, 1153-1179, 2008.

1 Snider, J. R., Guibert, S., Brenguier, J. L., and Putaud, J. P.: Aerosol activation in  
2 marine stratocumulus clouds: 2. Köhler and parcel theory closure studies, *Journal of*  
3 *Geophysical Research: Atmospheres* (1984–2012), 108, 2003.

4 Vogelmann, A. M., McFarquhar, G. M., Ogren, J. A., Turner, D. D., Comstock, J. M.,  
5 Feingold, G., Long, C. N., Jonsson, H. H., Bucholtz, A., and Collins, D. R.: RACORO  
6 extended-term aircraft observations of boundary layer clouds, *Bulletin of the*  
7 *American Meteorological Society*, 93, 861-878, 2012.

8 Wallace, J. M., and Hobbs, P. V.: *Atmospheric science: an introductory survey*,  
9 Academic press, 2006.

10 Wood, R., and Field, P. R.: The distribution of cloud horizontal sizes, *Journal of*  
11 *Climate*, 24, 4800-4816, 2011.

12 Zhao, G., and Di Girolamo, L.: Statistics on the macrophysical properties of trade  
13 wind cumuli over the tropical western Atlantic, *Journal of Geophysical Research:*  
14 *Atmospheres* (1984–2012), 112, 2007.

15

1    **Appendix A : The cloud model**

2    Unlike many parcel models in which the parcel's updraft is prescribed, in our  
3    theoretical analysis, we developed an air parcel model that is tuned to resolve the  
4    initiation of small buoyant air pockets that form due to weak perturbations in  
5    temperature or humidity. In order to account for the delicate processes that take  
6    place in the transition from haze to activated cloud droplets, the model solves the  
7    thermodynamic equations from first principles.

8    The core physics is based on the following equations that combine the vertical  
9    motion of a rising moist air parcel with the diffusional growth of humidified aerosols  
10   and water droplets within the parcel. All air parcel models implement some form of  
11   the first law of thermodynamics, usually as follows (Wallace and Hobbs, 2006):

12   A(1)                     $dT = \frac{1}{c_p} (dq + RT \frac{dp}{p}).$

13   (See Table A1 for a complete description of the symbols.)

14   Equation A(1) describes changes in the parcel temperature (dT); dT increases with  
15   the release of latent heat that occurs as water vapor condenses (dq) and cools as a  
16   result of the expansion of the parcel (RTdp/p). The latent heat released by  
17   inactivated haze droplets is incorporated into the model by means of a detailed  
18   scheme that treats the growth of humidified aerosols. The term dq is calculated by  
19   multiplying the change in mass of all the droplets (haze droplets and activated cloud  
20   droplets) with the latent heat. Namely

21   A(2)                     $dq = L_e \sum_{\text{all droplets}} dm$

22   Where  $dm(r) = 4/3\pi\rho(r^3 - (r - dr)^3)$  , and  $L_e = 10^3 \times (2500.8 - 2.36T +$   
23    $0.0016T^2 - 0.00006T^3)$  (for T in °C, Rogers, 1979). In order to simplify the model,

1 we neglected the effect of water vapor and liquid water on the specific heat ( $c_p$ ) and  
 2 used a constant value of dry air (Pruppacher and Klett, 1988).  
 3 The growth rate of every haze or cloud droplet is determined by a diffusion equation  
 4 that depends on the difference between the ambient relative humidity (or  
 5 supersaturation) in the air parcel ( $s_{v,w}$ ) and the relative humidity adjacent to the  
 6 droplet (Kohler, 1936). The growth rate also depends on the heat conductivity and  
 7 diffusion coefficients of the condensing water droplets. These relationships are  
 8 described by Pruppacher and Klett (1998) as follows:

9 A(3)

$$r \frac{dr}{dt} = \frac{D_v^* M_w e_{sat,w}(T_\infty)}{\rho_s'' \mathcal{R} T} (1 + s_{v,w} - \frac{1}{1 + \delta} \exp \left[ \frac{L_e M_w}{\mathcal{R} T} \left( \frac{\delta}{1 + \delta} \right) + \frac{2 M_w \sigma_{s/a}}{\mathcal{R} T (1 + \delta) \rho_w r} - \frac{v \Phi_s \varepsilon_m M_w \rho_N r_N^3}{M_s \rho_w (r^3 - r_N^3)} \right])$$

10 The rate of change of the supersaturation depends on two competing processes. The  
 11 supersaturation increases when the air parcel cools as it ascends and decreases  
 12 when vapor is depleted by the condensational growth of the haze and cloud droplets  
 13 (Lee and Pruppacher, 1977):

$$14 A(4) \frac{ds_{v,w}}{dt} = \frac{p}{\varepsilon e_{sat,w}} \frac{dw_v}{dt} - (1 + s_{v,w}) \left( \frac{\varepsilon L_e}{R_a T^2} \frac{dT}{dt} + \frac{g}{R_a T} U \right)$$

15 The second term on the right hand side of the equation represents the effect of the  
 16 adiabatic cooling on the saturation vapor pressure, while the third term represents  
 17 the effect of the expansion of the parcel on the vapor pressure.

18 The latter equation is derived under the assumptions that the partial pressure of the  
 19 dry air equals the pressure of the parcel, the density of the parcel equals the density  
 20 of dry air, and that  $dp/dt \approx -gpU$ .

21 The rate of change in the updraft of the parcel ( $U$ ) is derived from momentum  
 22 considerations (Lee and Pruppacher, 1977). A positive thermal contrast between the  
 23 parcel and the environment accelerates the parcel, while the drag force resulting  
 24 from the condensing water decelerates the parcel. The last term represents the

1 effect of the entrained air on the updraft. Since all the model's equations are  
2 coupled and the updrafts are small, this formalism represents reasonable treatment  
3 of the effect of the entrained air on the parcel motion (Pruppacher and Klett, 1998):

4 A(5) 
$$\frac{dU}{dt} = \frac{g}{1+\gamma} \left( \frac{T_v - T'_v}{T'_v} - W_L \right) - \mu_j U^2$$

5 The inputs to the model are the atmospheric profiles (temperature, relative humidity  
6 and pressure), the initial conditions of the parcel (vertical position, initial relative  
7 humidity, initial temperature and initial updraft) and the size distribution and  
8 chemical composition of the dry aerosol. The model calculates the temporal  
9 evolution of the vertical position, temperature, relative humidity, updraft and the  
10 size distribution of the growing water droplets of the parcel. The cloud base height  
11 was determined from the model results for a relative humidity level of 100 %. Since  
12 the model uses measured atmospheric profiles, the pressure is determined from  
13 the vertical position of the parcel at every time step.

14 In our model, the input data for the dry aerosol size distribution are based on  
15 number size distributions measured in Europe (Asmi et al, 2011). The distribution is  
16 represented by a discrete 250-bin parameterization sampled on a logarithmic scale.  
17 Because the influence of the size distribution of the aerosols on the cloud's  
18 properties greatly exceeds that of the chemistry of the aerosols (Reutter et al, 2009  
19 and Dusek et al, 2006), we assumed that all of the aerosols are ammonium sulfate;  
20 this assumption also allowed us to simplify the model. Furthermore, because the  
21 deliquescence relative humidity of ammonium sulfate is approximately 80 % (Brooks  
22 et al., 2002), we can assume that aerosols take up water vapor by diffusion in the  
23 very early stages of air parcel movement. To increase the accuracy of the model, we  
24 used a fine temporal resolution of 2.5 ms.

25 In addition we used measurements obtained by the Israeli Meteorological Service  
26 (IMS). The IMS station at Bet-Dagan is located 10 km east of the Mediterranean  
27 shore and measures the atmospheric profile on a daily basis by releasing a  
28 radiosonde at 12 UTC (15:00 local time during the summer). These sounding  
29 atmospheric profiles (website: atmospheric sounding) served two purposes: first,  
30 they were used as inputs for the air parcel model; and second, they were used to  
31 calculate the LCL. The LCL itself was derived by two different methods: 1) the

1 method used by the University of Wyoming (website: sounding station parameters  
 2 and indices), which uses the average value of the lower 500 m of the atmosphere  
 3 (referred to hereafter as the average LCL); and 2) a widely used approximation  
 4 described by Bolton (1980) and Stull (1988):

5 A(6) 
$$T_{LCL} = \frac{1}{\frac{1}{T_k - 55} - \frac{\ln(\frac{RH}{100})}{2840}} + 55$$

$$P_{LCL} = P \left( \frac{T_{LCL}}{T_k} \right)^{3.5}$$

6 where  $T_k$ ,  $P$  and  $RH$  are the temperature, pressure and relative humidity,  
 7 respectively, of the air parcel at the ground level (referred to hereafter as the ground  
 8 LCL).

9

10

11 Table A1 - List of symbols

Symbol	Quantity	Units
$T$	Air temperature inside the parcel	K
$q$	Latent heat release	$J \text{ kg}^{-1}$
$\mathcal{R}$	Gas constant for 1 mole of ideal gas	$J \text{ mole}^{-1} \text{ K}^{-1}$
$p$	Pressure	$J \text{ m}^{-3}$
$r$	Droplet radius	m
$D_v^*$	Modified diffusivity of water vapor in air	$\text{m}^2 \text{ s}^{-1}$
$M_w$	Molecular weight of water	$\text{mole}^{-1}$
$M_s$	Molecular weight of salt	$\text{mole}^{-1}$
$e_{sat,w}$	Saturation vapor pressure over a plane water surface	$J \text{ m}^{-3}$
$\rho_s''$	Density of aqueous salt solution	$\text{kg m}^{-3}$
$S_{v,w}$	Supersaturation of water vapor with respect to a plane water surface	Unitless
$\delta$	$= T_a / T_\infty - 1$	unitless
$L_e$	Latent heat of evaporation of pure water	$J \text{ kg}^{-1}$
$\sigma_{s/a}$	Surface tension of an aqueous solution drop against air	$J \text{ m}^{-2}$
$\rho_w$	Density of water	$\text{kg m}^{-3}$

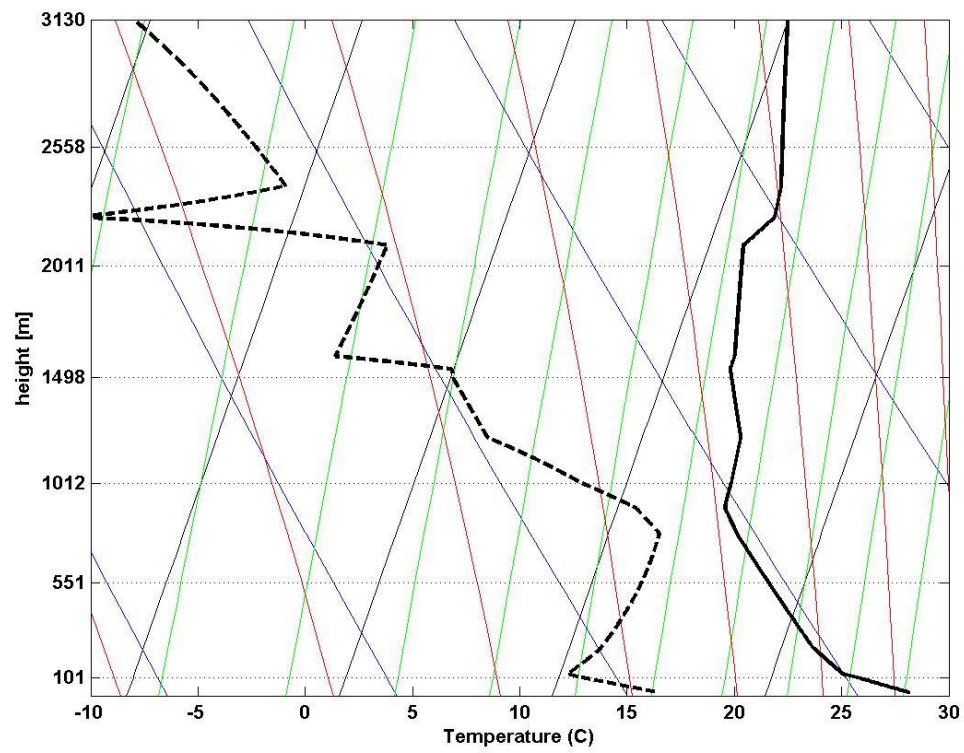
$v$	Number of ions into which a salt molecule dissociates in water	Unitless
$\Phi_s$	Osmotic coefficient	Unitless
$\rho_N$	Density of dry aerosol	$\text{kg m}^{-3}$
$r_N$	Radius of dry aerosol	m
$\varepsilon$	Molecular weight ratio of $\text{H}_2\text{O}$ to dry air (=0.622)	Unitless
$w_v$	Mixing ratio of water vapor	$\text{g g}^{-1}$
$R_a$	Gas constant for 1 g of dry air	$\text{J kg}^{-1} \text{K}^{-1}$
$g$	Acceleration of gravity	$\text{m s}^{-2}$
$U$	Vertical velocity of air parcel	$\text{m s}^{-1}$
$\gamma$	=0.5 correction for induced mass acceleration (Pruppacher and Klett, 1998)	unitless
$T_v$	Virtual temperature of air parcel	K
$T_v'$	Virtual temperature of environment	K
$W_L$	Liquid water mixing ratio in the air parcel	$\text{g}_{\text{water}} \text{g}_{\text{air}}^{-1}$
$\mu_J$	Entrainment rate for a convective plume	$\text{m}^{-1}$
$\varepsilon_m$	Mass fraction of water soluble substance in mixed aerosol particle	unitless
R	The universal gas constant	$\text{J K}^{-1} \text{mole}^{-1}$

1

2

3

4 **Appendix B: The atmospheric profile used in this study.**



1

2 **Figure. B1.** Tephigram of the atmospheric profile used in the model.

3